


cambridge.org/mrf

Aliakbar Dastranj , Ghazaleh Lari and Mosayeb Bornapour

Electrical Engineering Department, Faculty of Engineering, Yasouj University, Yasouj 75918-74831, Iran

## Industrial and Engineering Paper

**Cite this article:** Dastranj A, Lari G, Bornapour M (2021). A compact dual band-notched SWB antenna with high bandwidth dimension ratio. *International Journal of Microwave and Wireless Technologies* **13**, 87–93. <https://doi.org/10.1017/S1759078720000793>

Received: 30 October 2019

Revised: 15 May 2020

Accepted: 18 May 2020

First published online: 23 June 2020

### Key words:

Bandwidth dimension ratio (DBR); dual band-notched (DBN); super-wideband (SWB); WiMAX; WLAN

### Author for correspondence:

Aliakbar Dastranj,

E-mail: [dastranj@yu.ac.ir](mailto:dastranj@yu.ac.ir)

### Abstract

In this research, a compact dual band-notched (DBN) super-wideband (SWB) coplanar waveguide-fed antenna with high bandwidth (BW) dimension ratio of 7427.4 has been presented. The proposed antenna covers a very wide frequency range from 2.8 to 40 GHz (BW ratio of 14.28:1) with  $|S_{11}| < -10$  dB. The overall antenna size is  $20 \times 14 \times 1.6$  mm<sup>3</sup> which consists of an FR4 substrate with a dielectric constant of 4.4, a shovel-shaped radiating patch and the symmetric stair-shaped ground plane. The DBN characteristics are achieved by employing a pair of C-shaped and circular slots on its shovel-shaped radiating patch to reject the interferences caused by two WiMAX (3.7–4.7 GHz) and WLAN (5.7–6.4 GHz) bands. The notched frequency bands can be controlled by changing the radii of slots. The SWB property of the antenna is obtained by using a symmetric stair-shaped ground plane and also a shovel-shaped radiating patch. The measured results of the fabricated prototype in frequency- and time-domain are also presented and compared with the numerical results. The results indicate that the antenna has good performance over the entire operating BW (173.8%) which makes it very potential candidate for modern SWB applications.

### Introduction

Designing a compact size antenna with the most attractive characteristics such as low complexity, low cost, functioning over an extremely large impedance bandwidth (BW), high data rate and low interference in the modern wireless-enabled devices is a very challenging task, nowadays [1]. The ultra-wideband (UWB) planar monopole antenna with the allocated frequency spectrum of 3.1–10.6 GHz can be a good candidate to design in such communication systems [2]. However, as the demands for high data transmission is increasing, both short- and long-range frequency spectrum is needed. Super-wideband (SWB) technology is generally used for having BW ratio greater than 10:1 [3]. As this technology provides higher data rates and higher and more balanced BW, it can be used to send the data, voice, and video at higher speeds or ranging and monitoring applications, both in civil and military systems [4]. The SWB antenna can be found in very few papers because having an extremely large BW with stable radiation characteristic at higher frequencies is very challenging [5–11]. In [12], the antenna has a very large electrical dimension of  $0.45\lambda \times 0.45\lambda$  and BW of 1.0–19.4 GHz with a very low BW dimension ratio (BDR). In addition, the antenna presented in [13] has a BW ratio of 10.16:1 and the electrical dimension of  $0.47\lambda \times 0.32\lambda$  which is large in size compared to the BW the antenna provides.

A coplanar waveguide (CPW)-fed hexagonal Sierpinski fractal radiator for SWB applications with the electrical dimension of  $0.32\lambda \times 0.34\lambda$  is introduced in [14] which has a BW ratio of 11:1. In [15], a monopole antenna fed by microstrip line with a BW ratio of 13:1 and the electrical dimension of  $0.17\lambda \times 0.37\lambda$  has been proposed which has some radiation characteristic problems. The antenna presented in [16] has a low BDR due to its large electrical dimension of  $0.35\lambda \times 0.20\lambda$  compared to the BW of 3–35 GHz which the antenna can provide. Also, a set of SWB antennas were presented in [17–22] which will be compared to the proposed structure in the section “Measured results and discussion”.

The work presented in this research is a compact printed CPW-fed antenna ( $20 \times 14 \times 1.6$  mm<sup>3</sup>) with the electrical dimension of  $0.18\lambda \times 0.13\lambda$ , BW ratio of 14.28:1 and operating BW of 173.8%. The dual band-notched (DBN) characteristics are achieved by employing a pair of C-shaped and circular slots on its shovel-shaped radiating patch to reject the interferences caused by two WiMAX (3.7–4.7 GHz) and WLAN (5.7–6.4 GHz) bands. The notched frequency bands can be controlled by changing the radii of the slots. The SWB property of the antenna is obtained by using a symmetric stair-shaped ground plane and also a shovel-shaped radiating patch. The antenna has been simulated by full-wave Ansoft HFSS simulator package. The measured results of the fabricated prototype in frequency- and time-domain are also presented and compared with the simulated

results. The proposed antenna has a very good performance based on the achievement results in both simulation and measurement. The novelty of the proposed antenna lies in its simple structure, compact size, high BDR, and SWB operation along with DBN characteristics. The antenna design and the process of reaching the final structure will be discussed in the following sections.

### Antenna design

Different structures shown in Fig. 1 have been simulated and also analyzed by using HFSS which their comparison results of scattering parameter ( $|S_{11}|$ ) curves are illustrated in Fig. 2. First of all, a simple rectangular radiating patch with a rectangular feed line and a rectangular finite ground plane has been considered in structure 1 which is not appropriate for SWB or even UWB applications due to its low impedance BW. Consequently, a shovel-shaped radiating patch is designated in structure 2 to make the impedance BW a little wider which is useful for UWB applications. Subsequently, it can be seen in structure 3, the chosen symmetric stair-shaped ground plane instead of a rectangular one so that the entire SWB operating range of 2.8–40 GHz is achieved. As was investigated in previous works [23, 24], the leaky-wave interaction between the ground plane and radiator can affect the impedance matching of the antenna. Lower leaky-wave from the ground plane and radiator leads to a better impedance matching and, hence, broadband characteristic for the antenna. The symmetric stair-shaped section decreases the leakage current distribution from the ground plane. As a result, the antenna performance becomes better [23, 24]. Figure 3 illustrates the process of reaching DBN characteristics of the SWB antenna. As can be seen in Fig. 3(a), no slots have been etched on the radiating patch of the antenna. The band-notched characteristic of WiMAX band (3.7–4.7 GHz) which is the first band stop (BS) can be generated by etching a C-shaped slot on the shovel-shaped radiating patch in Fig. 3(b). It is shown that in Fig. 3(c) the second BS characteristic (WLAN (5.7–6.4 GHz)) can be generated by employing another C-shaped slot with smaller size radius. The final structure of the proposed antenna is shown in Fig. 3(d). In order to have a SWB antenna with DBN characteristics, two C-shaped slots and a circular slot have been etched on its radiating patch. The simulated scattering parameters ( $|S_{11}|$ ) of the structures 1–3 and the final structure are compared in Fig. 4. This figure clearly shows BW enhancement process and DBS characteristics of the antenna. As it can be observed from this figure, the final structure can reject unwanted frequencies at WiMAX and WLAN band stops. The geometry of the final optimized SWB DBN antenna with detailed and necessary dimensions that affect the impedance BW and DBN characteristics is shown in Fig. 5. Optimization of the dimensions has been accomplished by using HFSS software package. The antenna is compact which is printed on FR4 substrate with permittivity 4.4 and loss tangent of 0.02. The optimal dimensions (in mm) of the proposed antenna are as follows:  $W = 14$ ,  $L = 20$ ,  $h = 1.6$ ,  $W_f = 1.5$ ,  $L_g = 8$ ,  $L_{gn} = 7.5$ ,  $W_1 = 1$ ,  $W_2 = 0.8$ ,  $W_3 = 0.47$ ,  $W_4 = 3.48$ ,  $L_1 = 4.8$ ,  $L_2 = 6.05$ ,  $L_3 = 6.7$ ,  $L_4 = 4.6$ , and  $g = 0.5$ . Important dimensions (in mm) which affect the DBN characteristics as shown in Fig. 5(b) respectively are:  $r1 = 4.6$ ,  $r2 = 4.1$ ,  $r3 = 3.3$ ,  $r4 = 2.8$ , and  $r5 = 1.12$ . The radii of the slots can be calculated approximately from the following formula. In these equations,  $f_{notch1}$  and  $f_{notch2}$  are the center frequencies of

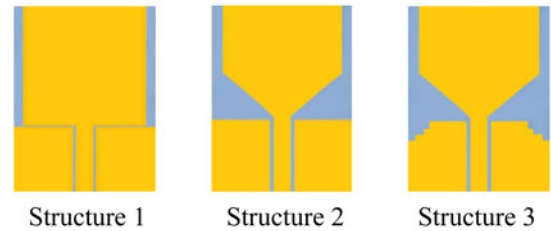


Fig. 1. Impedance BW enhancement process.

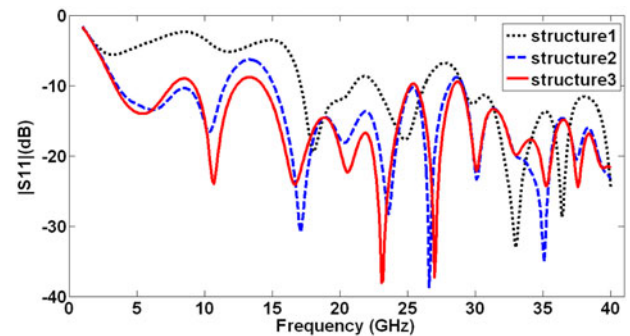


Fig. 2. Comparison of the input impedance matching curves for three structures.

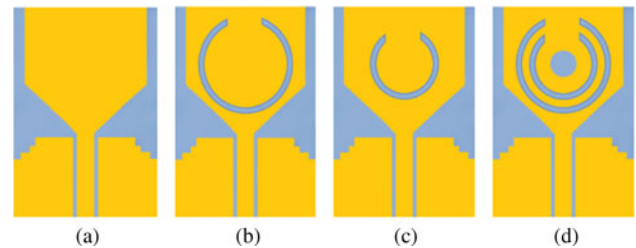


Fig. 3. (a) antenna structure without slots, (b) C-shaped slot used for WiMAX BS, (c) C-shaped slot used for WLAN BS, and (d) final structure.

the rejected WiMAX (3.7–4.7 GHz) and WLAN (5.7–6.4 GHz) bands and  $c$  is the light speed at free space [25].

$$r_{WiMAX} = \frac{c}{f_{notch1} \times 4 \times \sqrt{\epsilon_{eff}} \times 2\pi \times 0.64}, \quad (1)$$

$$r_{WLAN} = \frac{c}{f_{notch2} \times 4 \times \sqrt{\epsilon_{eff}} \times 2\pi \times 0.64}, \quad (2)$$

$$\epsilon_{eff} = \frac{\epsilon_r + 1}{2}. \quad (3)$$

As a parametric study of DBN characteristics of the proposed antenna, different values of  $r2$ ,  $r3$ ,  $r4$ , and  $r5$  are considered to see their effects on band rejection in both WLAN and WiMAX. It can be concluded from Table 1 that  $r2$  has an effect on first BS (WiMAX) while Table 2 indicates that  $r4$  has an effect on the second BS, WLAN band. However, in Table 3, as it can be observed  $r3$  effects both WiMAX and WLAN bands. Effects of  $r5$  variation on the band rejection behavior of the antenna are tabulated in Table 4. This table shows that the circular slot in

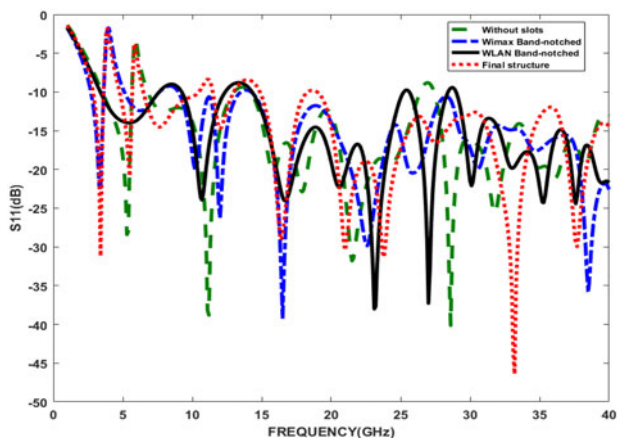


Fig. 4. Scattering parameter ( $|S_{11}|$ ) simulation results of the structures mentioned in Fig. 3.

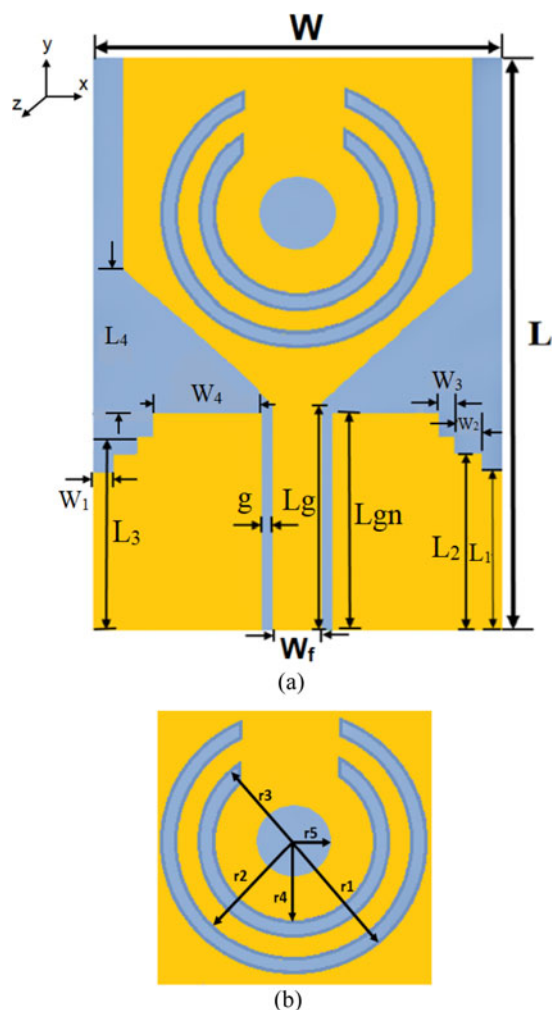


Fig. 5. (a) Geometry of the proposed antenna, (b) important parameters which affect the antenna's DBN characteristic.

the center of the patch affects band rejection in both WLAN and WiMAX bands. The best values of the parameters achieved by optimization via HFSS simulator package are summarized as follows (in mm):  $r_2 = 4.1$ ,  $r_3 = 3.3$ ,  $r_4 = 2.8$ , and  $r_5 = 1.12$ .

Table 1. Effects of  $r_2$  on the first and second band stops

Band	Band 1 (WiMAX)		Band 2 (WLAN)	
	$F_{L1}$ (GHz)	$F_{H1}$ (GHz)	$F_{L2}$ (GHz)	$F_{H2}$ (GHz)
$r_2 = 3.5$	4.1	4.9	5.7	6.2
$r_2 = 4.1$	3.7	4.7	5.7	6.4
$r_2 = 4.3$	3.5	4.4	5.7	6.4

Table 2. Effects of  $r_4$  on the first and second band stops

Band	Band 1 (WiMAX)		Band 2 (WLAN)	
	$F_{L1}$ (GHz)	$F_{H1}$ (GHz)	$F_{L2}$ (GHz)	$F_{H2}$ (GHz)
$r_4 = 1.8$	3.7	4.7	6.8	7.6
$r_4 = 2.2$	3.7	4.7	6.5	7.2
$r_4 = 2.8$	3.7	4.7	5.7	6.4

Table 3. Effects of  $r_3$  on the first and second band stops

Band	Band 1 (WiMAX)		Band 2 (WLAN)	
	$F_{L1}$ (GHz)	$F_{H1}$ (GHz)	$F_{L2}$ (GHz)	$F_{H2}$ (GHz)
$r_3 = 2.9$	3.7	4.9	6.4	6.8
$r_3 = 3.3$	3.7	4.7	5.7	6.4
$r_3 = 3.7$	3.7	4.4	5.3	6.3

Table 4. Effects of  $r_5$  on the first and second band stops.

Band	Band 1 (WiMAX)		Band 2 (WLAN)	
	$F_{L1}$ (GHz)	$F_{H1}$ (GHz)	$F_{L2}$ (GHz)	$F_{H2}$ (GHz)
$r_5 = 1.1$	3.8	5.0	6.3	6.9
$r_5 = 1.12$	3.7	4.7	5.7	6.4
$r_5 = 1.14$	3.8	4.6	5.4	6.4

In this design, to achieve super-wideband operation from 2.8 to 40 GHz with high BW dimension ratio of 7427.4 and dual band-notched characteristics, other methods such as using split-ring resonators and metamaterials were examined. Based on the numerous simulations, the aforementioned characteristics were not achieved by these techniques. However, using C-shaped and circular slots lead to super-wide BW without interferences by WiMAX and WLAN bands.

The Comparison of  $|S_{11}|$  parameters for the antennas printed on RT Duroid (with rescaled dimensions) and FR4 substrates is presented in Fig. 6. Notice that the relative permittivity values of FR4 and RT Duroid substrates are 4.4 and 2.2, respectively. Accordingly, a ratio of the square of 2 was taken in rescaling

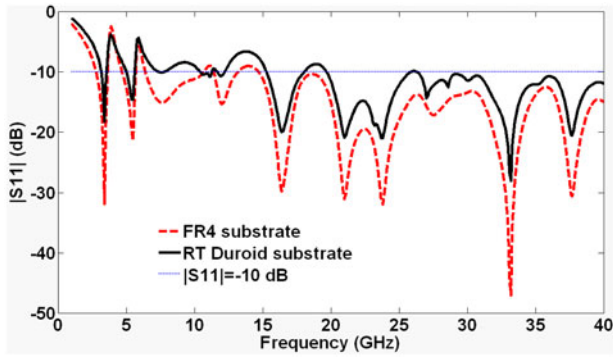


Fig. 6. Comparison of  $|S_{11}|$  parameters for the antennas printed on RT Duroid and FR4 substrates.

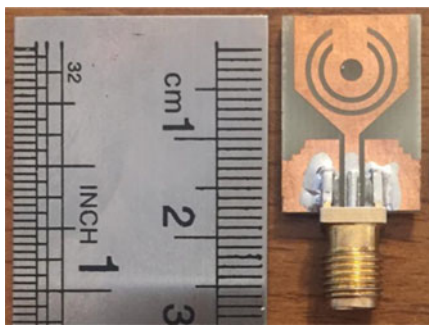


Fig. 7. Photograph of the proposed antenna prototype.

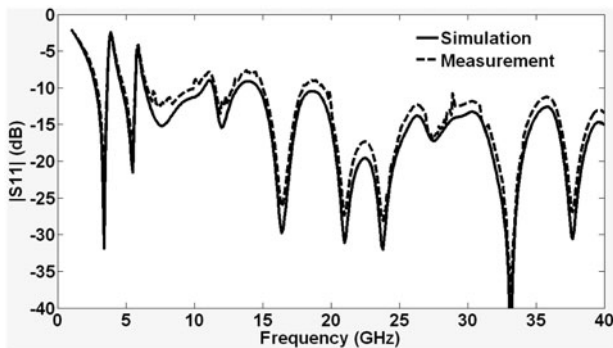


Fig. 8. Comparison between the numerical and experimental  $|S_{11}|$  curves of the antenna.

the antenna dimension for the RT Duroid material. It is seen that the antenna with RT Duroid substrate has  $|S_{11}| > -10$  dB over the large part of the desired band. Therefore, the antenna was printed on FR4 substrate. It should be noted that the worst input matching realized using RT Duroid substrate could be partially due to the lower losses of this substrate. In other words, the higher losses of FR4 are certainly a bad factor for the antenna gain, but they may play a good part to improve the input matching.

**Measured results and discussion**

Figure 7 shows the photograph of the proposed antenna prototype. The antenna was simulated by using HFSS software package.

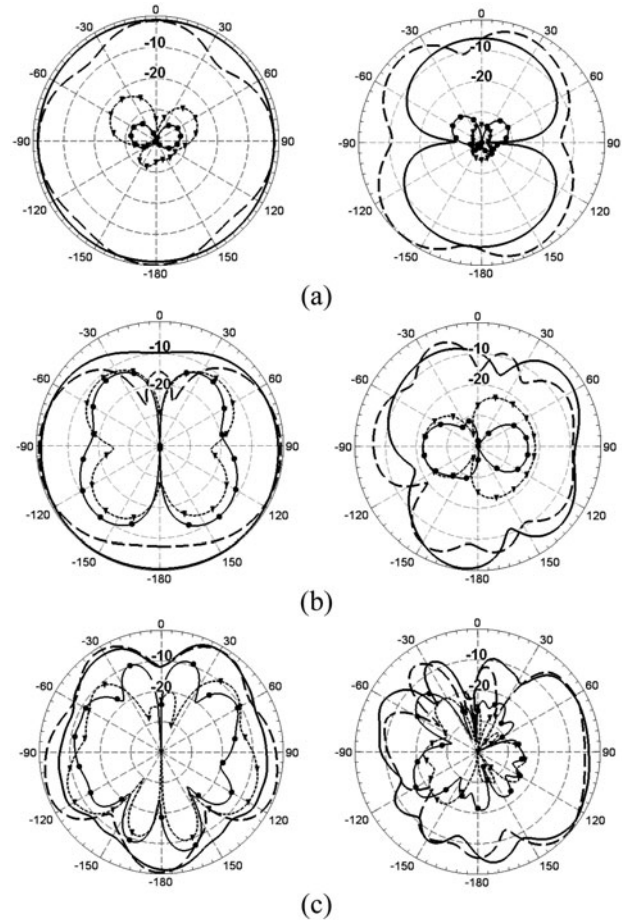


Fig. 9. Experimental and numerical far-field  $E$  ( $y$ - $z$ ) and  $H$  ( $x$ - $z$ ) plane patterns of the antenna (left:  $x$ - $z$  plane, right:  $y$ - $z$  plane) at (a) 3 GHz, (b) 18 GHz, and (c) 40 GHz.

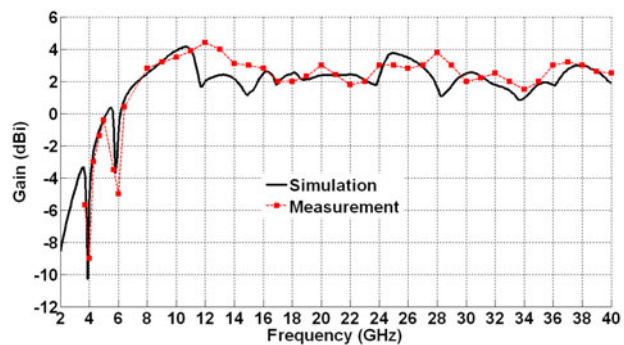


Fig. 10. Numerical and experimental gain of the antenna versus frequency.

Then, it was fabricated to validate the results which are carried out by simulation. The designed antenna is connected to a 50-ohm SMA connector for signal transmission. The part number of SMA female connector is SC8026 which normally operates from DC up to a frequency of 18 GHz and offers excellent

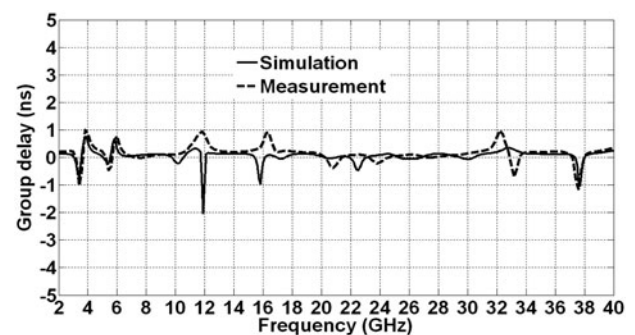
**Table 5.** Comparison of the proposed antenna with other SWB antennas (AG, average gain, GD, group delay). Note that the electrical dimension and the BDR are calculated at the wavelength at the lower cut-off frequency of the working BW

Ref.	Electrical dimension ( $\lambda^2$ )	BDR	$\epsilon_r$	BW ratio	AG (dBi)	GD (ns)
[11]	$0.27 \times 0.23$	2541.12	4.4	10.00:1	3.4	<0.7
[12]	$0.45 \times 0.45$	890.83	4.4	19.40:1	0.94	–
[13]	$0.47 \times 0.32$	1102.91	3.24	10.16:1	–4.8	–
[14]	$0.32 \times 0.34$	1531.89	4.4	11.00:1	6.1	–
[15]	$0.17 \times 0.37$	2735.00	4.4	13.06:1	4.1	–
[16]	$0.35 \times 0.20$	2400.00	2.2	11.60:1	5.8	–
[17]	$0.23 \times 0.32$	2230.00	–	10.31:1	3.3	–
[18]	$0.41 \times 0.29$	1347.24	3.38	9.11:1	2.93	<1
[19]	$0.44 \times 0.44$	905.00	3.0	13.63:1	–	–
[20]	$2.00 \times 2.00$	33.33	4.5	5.00:1	3.4	–
[21]	$0.32 \times 0.34$	1682.00	2.65	25.00:1	4.9	<5
[22]	$0.43 \times 0.45$	950.77	3.48	25.00:1	4.5	–
Proposed	$0.18 \times 0.13$	7427.40	4.4	14.28:1	2.96	<2

VSWR of 1.23:1. However, this connector features VSWR of about 1.45:1 for the frequency range of 18–40 GHz. It is a low lost connector with reasonable lose.

### Frequency-domain results

Measured scattering parameter ( $|S_{11}|$ ) comparing with the simulated one is shown in Fig. 8. There is a negligible difference between the simulated and measured results. As shown in this figure, the measured scattering parameter at some part of the frequency between 10 and 16 GHz goes greater than  $-10$  dB. This is due to the measurement errors, fabrication tolerances, and SMA soldering effects. Hence, good agreement between measured and simulated results has been achieved which means the antenna is a very good candidate for SWB applications with DBN property. However, in order to further understand the utility of the proposed antenna over the entire operating BW, other radiation characteristics such as far-field patterns and gain must also be carefully investigated. The far-field radiation patterns of the SWB antenna in  $H$  ( $x$ - $z$ )- and  $E$  ( $y$ - $z$ )-plane at several frequencies were measured. For brevity, results at the lower band edge frequency (3 GHz), mid-frequency (18 GHz), and higher band edge frequency (40 GHz) are presented and compared with simulated ones (Fig. 9). As can be observed from Fig. 9(a), the antenna has an omnidirectional pattern in  $H$ -plane and bidirectional pattern in the  $E$ -plane at low frequencies with very low cross-polarization level. Figures 9(b) and (c) show that the radiation patterns at higher frequencies are also reasonable. Notice that the cross-polarization level increases at higher frequencies due to excitation of higher-order modes. Notice that input matching and antenna gain are promising even beyond higher band edge frequency. However, at the frequencies higher than 40 GHz, the radiation patterns in both  $E$ - and  $H$ -plane start deteriorating. Also, cross-polarization significantly increases at these frequencies. Thus, the operation BW of the antenna is restricted by the increasing deterioration of the radiation patterns and the increasing cross-polarization at the higher frequencies.

**Fig. 11.** Comparison between the experimental and numerical group delay results of the antenna versus frequency.

The simulated and measured peak gain curves of the antenna versus frequency are illustrated in Fig. 10. Due to the omnidirectional behavior of the antenna in  $x$ - $z$  plane, the direction of the peak gain is not stable. As shown in this figure, the antenna gain sharply drops at the center frequencies of WiMAX and WLAN band stops (4 and 6 GHz). As plotted in Fig. 10, the measured gain at the notch frequencies of the band stops, i.e., 3.7, 4, 4.3, 4.7, 5.7, 6, and 6.4 GHz is  $-5.7$ ,  $-9$ ,  $-3$ ,  $-1.4$ ,  $-3.5$ ,  $-5$ , and  $0.42$  dBi, respectively. Note that the measured gain is moderate at the operating frequency band respecting the small size of the antenna.

In SWB antennas, BDR is an important parameter that the higher BDR signifies wider frequency band and compactness of the proposed antenna compared to the other structures. BDR indicates how much operating BW (in percentage) can be provided per electrical area unit. Equality is defined as follows [15]:

$$BDR = \frac{BW(\%)}{\lambda_{Length} \times \lambda_{Width}} \quad (4)$$

In this equation,  $\lambda$  is the wavelength at the lower cut-off frequency of the working BW. The results of the comparison between the designed antenna and other antenna structures studied in [11–22], are presented in Table 5 on the basis of

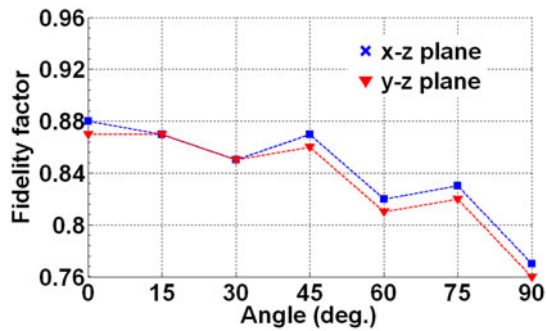


Fig. 12. Calculated fidelity factor of the antenna.

BDR. In spite of the small electrical dimension of the proposed antenna compared to the others, a large BDR of 7427.4 is exhibited. Accordingly, it can be concluded that the proposed SWB antenna can provide good BW ratio and very larger BDR characteristics with a much smaller size in comparison to the other antennas.

### Time-domain results

Along with the frequency-domain analysis, time-domain performance should also be analyzed in order to be sure of the SWB operation [26, 27]. The time-domain analysis required two identical designed antennas, one as the transmitter and the other one as a receiver, in the adjustment of face-to-face and side-by-side. Time-domain analysis of both configurations was considered using CST Microwave Studio by a distance of 50 cm. Time taken by the antenna to receive the pulse is indicated by an important parameter named group delay. Group delay of face-to-face orientation is shown in Fig. 11 which its peak-to-peak variation is less than 2 ns over the entire frequency band. Although the result of the side-by-side configuration has not been discussed in this section, similar results were obtained which indicate an acceptable time-domain performance.

Another important parameter in time-domain analysis named the fidelity factor is used to calculate the correlation between transmitted and received pulses. By using the approach suggested in [28], the input signal is delivered to the antenna, and the far-field electric component is received by means of four virtual probes. To investigate the fidelity factor in both  $E$ - and  $H$ -plane, seven probes are placed at the angle equal to 0°, 15°, 30°, 45°, 60°, 75°, and 90°. Figure 12 presents this time-domain parameter for both planes. In a typical UWB system, the values of fidelity factor can vary between 0 and 100%. A fidelity factor value of 0% shows that the received and input pulses are completely different from each other, while a value of 100% indicates that the received and input signals are perfectly similar. As was mentioned in [26], a fidelity factor higher than 50% is the appropriate value for UWB systems. From Fig. 12, it is seen that the fidelity factor in both planes has acceptable values greater than 76%, making the proposed antenna very capable for use in SWB communication applications.

### Conclusion

A compact SWB antenna with an electrical dimension of  $0.18 \lambda \times 0.13 \lambda$ , BW ratio of 14.28:1 and operating BW of 173.8% was proposed in this work. To achieve SWB operation, symmetric stair-

shaped ground plane, and a shovel-shaped radiating patch instead of rectangular one was chosen. In order to reject the interferences caused by two WiMAX (3.7–4.7 GHz) and WLAN (5.7–6.4 GHz) bands, a pair of C-shaped and circular slots were etched on the shovel-shaped radiating patch. It was shown that the notched frequency bands can be controlled by changing the radii of the slots. The measured results of the fabricated prototype in frequency- and time-domain were also presented and compared with the simulated results. The antenna has a very good performance based on the achievement results in both simulation and measurement. The proposed antenna has several advantages such as simple structure, compact size, high BDR, and SWB operation along with DBN characteristics. Based on the aforementioned advantages, the antenna is an excellent radiating element for SWB communication systems.

### References

1. Samsuzzaman M and Islam MT (2015) A semicircular shaped super wideband patch antenna with high bandwidth dimension ratio. *Microwave and Optical Technology Letters* 57, 445–452.
2. Okas P, Sharma A, Das G and Gangwar RK (2018) Elliptical slot loaded partially segmented circular monopole antenna for super wideband application. *International Journal of Electronics and Communications* 88, 63–69.
3. Bernety HM, Zakeri B and Gholami R (2011) Design of a novel directional microstrip-fed super-wideband antenna. *Modares Journal of Electrical Engineering* 11, 2563–2570.
4. Okas P, Sharma A and Gangwar RK (2018) Super wideband CPW-fed modified square monopole antenna with stabilized radiation characteristics. *Microwave and Optical Technology Letters* 60, 568–575.
5. Manohar M, Kshetrimayum RS and Gogoi AK (2014) Printed monopole antenna with tapered feed line, feed region and patch for super wideband applications. *IET Microwaves, Antennas and Propagation* 8, 39–45.
6. Balani W, Sarvagya M, MM T, Ali MP, Anguera J, Andujar A and Das S (2019) Design techniques of super-wideband antenna-existing and future prospective. *IEEE Access* 7, 141241–141257.
7. Awan WA, Zaidi A and Baghdad A Super wide band miniaturized patch antenna design for 5G communications. *International Conference on Wireless Technologies, Embedded and Intelligent Systems, 3–4 April 2019, Fez, Morocco, Morocco*.
8. Alluri S and Rangaswamy N A super wideband circular monopole antenna. *International Conference on Microwave Integrated Circuits, Photonics and Wireless Networks (IMICPW), 22–24 May 2019, Tiruchirappalli, India, India*.
9. Chu S, Hasan MN, Yan J and Chu CC A planar super wideband annular ring monopole antenna with time domain characterization. *Asia-Pacific Microwave Conference (APMC), 6–9 November 2018, Kyoto, Japan*.
10. Kwon OH, Park WB, Lee S, Lee JM, Park YM and Hwang KC Super-wideband spidron fractal cube antenna using 3D printing technology. *International Symposium on Antennas and Propagation (ISAP), 23–26 October 2018, Busan, Korea (South), Korea*.
11. Singhal S and Singh AK (2016) CPW-fed phi-shaped monopole antenna for super wide-band applications. *Progress in Electromagnetics Research* 64, 105–116.
12. Yeo J and Lee JI (2014) Coupled-sectorial-loop antenna with circular sectors for super wideband applications. *Microwave and Optical Technology Letters* 60, 1683–1689.
13. Hakimi S, Rahim SKA, Abedian M, Noghbaei S, Khalily M and Singh AK (2016) CPW-fed transparent antenna for extended ultrawideband applications. *IEEE Antennas and Wireless Propagation Letters* 10, 1701–1707.
14. Singhal S and Singh AK (2014) CPW-fed hexagonal Sierpinski super wideband fractal antenna. *IET Microwaves, Antennas and Propagation* 8, 39–45.

15. **Chen KR, Sim C and Row JS** (2011) A compact monopole antenna for super wideband applications. *IEEE Antennas and Wireless Propagation Letters* **10**, 488–491.
16. **Shahu BL, Pal S and Chatteraj N** (2015) Design of super wideband hexagonal-shaped fractal antenna with triangular slot. *Microwave and Optical Technology Letters* **57**, 1659–1662.
17. **Deng C, Xie YJ and Li P** (2009) CPW-fed planar printed monopole antenna with impedance bandwidth enhanced. *IEEE Antennas and Wireless Propagation Letters* **8**, 1394–1397.
18. **Srifi MN, Podilchak SK, Essaïdi M and Antar YMM** (2011) Compact disc monopole antennas for current and future ultrawideband (UWB) applications. *IEEE Transactions on Antennas and Propagation* **59**, 4470–4480.
19. **Cheng S, Hallbjörner P and Rydberg A** (2008) Printed slot planar inverted cone antenna for ultrawideband applications. *IEEE Antennas and Wireless Propagation Letters* **7**, 18–21.
20. **Azari A** (2011) A new super wideband fractal microstrip antenna. *IEEE Transactions on Antennas and Propagation* **59**, 1724–1727.
21. **Dong Y, Hong W, Liu L, Zhang Y and Kuai Z** (2009) Performance analysis of a printed super wideband antenna. *Microwave and Optical Technology Letters* **51**, 949–956.
22. **Liu J, Esselle KP, Hay SG and Zhong S** (2011) Achieving ratio bandwidth of 25:1 from a printed antenna using a tapered semi-ring feed. *IEEE Antennas and Wireless Propagation Letters* **10**, 1333–1336.
23. **Dastranj A** (2017) Very small planar broadband monopole antenna with hybrid trapezoidal-elliptical radiator. *IET Microwaves, Antennas & Propagation* **11**, 542–547.
24. **Dastranj A** (2017) Low-profile ultra-wideband polarisation diversity antenna with high isolation. *IET Microwaves, Antennas & Propagation* **11**, 1363–1368.
25. **Liu HW, Ku CH and Yang CF** (2010) Novel CPW-Fed planar monopole antenna for WiMAX/WLAN applications. *IEEE Transactions on Antennas and Propagation* **9**, 240–243.
26. **Quintero G, Zurcher JF and Skrivervik AK** (2011) System fidelity factor: a new method for comparing UWB antennas. *IEEE Transactions on Antennas and Propagation* **59**, 2502–2512.
27. **Weisbeck W, Adamiuk G and Sturm C** (2009) Basic properties and design principles of UWB antennas. *Proceedings of the IEEE* **97**, 372–385.
28. **Wu Q, Jin R, Geng J and Ding M** (2007) Pulse preserving capabilities of printed circular disk monopole antennas with different grounds for the specified input signal forms. *IEEE Transactions on Antennas and Propagation* **55**, 2866–2873.



**Aliakbar Dastranj** was born in Yasouj, Iran, in 1983. He received the B.S. degree in Electronics Engineering from Shiraz University, Shiraz, Iran, in 2006, the M.S. degree in Electrical and Communications Engineering from Shahed University, Tehran, Iran, in 2008, and the Ph.D. degree in Electrical and Communications Engineering from Shiraz University, Shiraz, Iran, in 2013. From 2008 to

2013 he was a research fellow at the School of Electrical and Computer

Engineering, Shiraz University. In 2014, he joined the Department of Electrical Engineering, Yasouj University, Yasouj, Iran, as an Assistant Professor, where he has been an Associate Professor since 2018. His research interests include novel designs of modern antennas for advanced applications, design and modeling of microwave structures, evolutionary algorithms for electromagnetic applications, and electromagnetic theory. He has published more than 60 papers in peer-reviewed international journals and conference proceedings.



**Ghazaleh Lari** was born in Shiraz, Iran in 1996.

She received the B.Sc. degree in electrical engineering from Yasouj University, Yasouj, Iran in 2018, and is working toward the M.Sc. degree in telecommunication engineering at the Middle East Technical University, Ankara, Turkey. Her research interest is analyzing and designing microstrip antennas and she has participated in some projects relative to design and

modeling of microwave structures and antenna designing.



**Mosayeb Bornapour** was born in 1988. He got his bachelor degree in the field of electrical power engineering in July, 2010 from the University of Rajaei in Tehran. He got first rank in his undergraduate season. He earned his master degree in the field of electrical power engineering in January, 2013 from Shiraz University of technology and he received his Ph.D. degree in the field of electrical power engineering in

August, 2017 from University of Isfahan. Since September 2017, he is Assistant Professor of Electrical Engineering Department of Yasouj University. His research interest includes Optimal Operation and Planning of Power Systems; Optimization in Distribution Networks; Distributed Generations (Fuel Cell Power Plant, Wind Turbines, Photovoltaic); Combined Heat and Power (CHP); Reliability Evaluation of Power Systems; Electrical Market; Micro Grid; Optimization methods in power systems and distribution networks; Evolutionary Algorithms; Stochastic Methods. He has published more than 30 papers in peer-reviewed international journals and conference proceedings.